EEET ECOLOGICAL ENGINEERING & ENVIRONMENTAL TECHNOLOGY

Ecological Engineering & Environmental Technology, 2026, 27(6), 135–152
https://doi.org/10.12912/27197050/221291
ISSN 2719–7050, License CC-BY 4.0

Received: 2026.04.06
Accepted: 2026.05.15
Published: 2026.06.01

Engineering high-performance activated carbons from plum pit shells for efficient copper(II) removal: Synthesis, structural characterization, and adsorption mechanisms

Dilnoza Salikhanova[1], Mirtokhir Muratov[1*], Zulfiya Usmonova[2], Aziza Abdikamalova[1], Izzat Eshmetov[1], Dilnoza Jumayeva[1], Dilafruz Sagdullayeva[3], Mukhtasar Ismoilova[1,2], Nafisa Qodirova[4], Rasulbek Eshmetov[5]

[1] Institute of General and Inorganic Chemistry, Academy of Sciences of Republic of Uzbekistan, 77a M. Ulugbek, 100170, Uzbekistan
[2] Namangan State Technical University, Namangan, Uzbekistan
[3] Institute of Bioorganic Chemistry, Academy of Sciences of the Republic of Uzbekistan, Tashken, Uzbekistan
[4] Fergana Polytechnic Institute, Fergana, Uzbekistan
[5] Mamun University, Khorezm, Uzbekistan
* Corresponding author's e-mail: muratovmirtoxir@mail.ru

ABSTRACT

This study aims to develop high-performance carbon adsorbents from plum pit shells and to evaluate the relationship between synthesis conditions, structural evolution, and Cu(II) adsorption performance in aqueous systems. The work addresses the valorization of agricultural waste into functional porous carbon materials suitable for environmental remediation applications. Plum pit shells were converted into carbon materials through controlled pyrolysis followed by KOH chemical activation. The influence of carbonization temperature, activation ratio, and thermal treatment conditions on material structure was systematically investigated. The resulting materials were characterized using SEM, XRD, FTIR, TGA, and nitrogen adsorption-desorption analysis, while adsorption behavior toward Cu(II) ions was evaluated through batch experiments under varying operational parameters, including pH, adsorbent dosage, contact time, and temperature. Equilibrium, kinetic, and thermodynamic models were applied to describe the adsorption process. The results showed that the optimized activated carbon achieved a specific surface area of up to 944.25 m^2/g at a KOH-to-biochar ratio of 1:0.05. Cu(II) removal efficiency reached approximately 95% under optimal conditions (pH 5–6, 1.5–2.0 g/L dosage, 60–90 min contact time). Adsorption data were well described by the Langmuir model ($R^2 > 0.99$), indicating predominantly monolayer adsorption. Thermodynamic analysis confirmed that the process is spontaneous and exothermic, with negative Gibbs free energy values across the studied temperature range. The initial hypothesis regarding the formation of highly porous carbon structures and their strong affinity for Cu(II) ions was confirmed. A limitation of this study is that adsorption performance was evaluated using synthetic aqueous solutions rather than real wastewater systems, and regeneration cycles were not experimentally validated. Nevertheless, the materials demonstrate strong potential for practical water treatment applications. The practical value of this work lies in transforming low-cost agricultural waste into efficient adsorbents for heavy metal removal, contributing to sustainable water purification technologies. The originality of the study is in the systematic correlation of KOH activation parameters with pore development and adsorption performance for plum pit-derived carbon, an underexplored biomass precursor. The findings provide new insights into biomass-derived carbon design and support circular economy strategies for waste-to-material conversion.

Keywords: plum pit shells, carbon adsorbents, KOH activation, microporous structure, sustainability.

INTRODUCTION

Rapid industrialization and population growth have intensified the discharge of hazardous contaminants into aquatic systems, including heavy metal ions, dyes, and organic pollutants, posing significant risks to ecosystems and human health (Muratov et al., 2024). Conventional water treatment technologies such as chemical precipitation, membrane filtration, and ion exchange are widely applied; however, they often suffer from limitations including high operational costs, secondary waste generation, and energy demand. Among available alternatives, adsorption remains one of the most efficient and operationally simple approaches for contaminant removal, particularly when using porous carbon-based materials.

Activated carbon is extensively used as an adsorbent due to its high surface area and tunable porosity. However, its large-scale production is still predominantly based on non-renewable precursors such as coal and petroleum-derived feedstocks, which limits its sustainability and increases environmental burden (Khoshimov et al., 2025). In recent years, biomass-derived carbons have attracted increasing attention as sustainable alternatives, offering low cost, renewable sourcing, and waste valorization potential. Agricultural residues such as nutshells, fruit pits, and shells are particularly promising due to their high carbon content and lignocellulosic structure.

Among agricultural wastes, fruit pit shells represent an underutilized biomass fraction with potential for carbon material production. Plum pits are generated in large quantities by the fruit processing industry, and their disposal presents both environmental and economic challenges. Their relatively high fixed carbon content and rigid structure make them suitable precursors for activated carbon synthesis. However, despite extensive studies on other fruit-derived biomasses such as apricot, cherry, and walnut shells, systematic investigation of plum pit shell-derived activated carbon remains limited, particularly in terms of controlled synthesis–structure–performance relationships.

Although biomass-derived activated carbons have been widely investigated, several key scientific gaps remain. First, the influence of combined carbonization and chemical activation parameters on the development of pore structure in plum pit-derived carbons has not been systematically studied. Second, the relationship between activation conditions, surface chemistry, and heavy metal adsorption performance remains insufficiently understood for this precursor. Third, quantitative evaluation of adsorption behavior, including equilibrium, kinetics, and thermodynamics for Cu(II) removal using plum pit-derived carbons, is still limited in the literature.

Over the years, researchers have explored biomass-derived materials for activated carbon production, including coconut shells, corn cobs, rice husks, walnut shells, and sawdust. Different activation methods, including physical (steam and CO_2) and chemical (acid and base) activation, have been employed to enhance the porosity and adsorption capacity of carbon adsorbents. In this process, using KOH, H_3PO_3, and $ZnCl_2$ has been highly efficient at generating high-surface-area carbons featuring optimised porosity (Arami-Niya et al., 2010).

Despite these advancements, research on plum pit shells as a starting material for activated carbon remains limited. Some studies have investigated the thermal and chemical treatment of fruit pit shells, including apricot and cherry, but comprehensive studies on the optimisation of plum pit shell activation processes, structural characterisation, and application potential in environmental remediation are lacking. Furthermore, there is a need for systematic investigations into the effects of activation parameters on adsorption property, and comparison with conventional activated carbons.

Despite the progress in biomass-based activated carbon research, several knowledge gaps remain. First, there is limited information on the optimal processing conditions for converting plum pit shells into high-performance carbon adsorbents. The influence of different operational factors, including thermal input, activation agent concentration, activation time, on the textural and chemical properties of the resulting adsorbents has not been fully explored. Additionally, although studies have reported the adsorption capacities of bio-based carbons, comprehensive evaluations of their adsorption mechanisms, kinetics, and thermodynamics for various pollutants remain lacking (Neme et al., 2022). Moreover, the long-term stability, reusability, and regeneration potential of plum pit shell-derived adsorbents remain unassessed. Addressing these gaps will provide valuable insights into the feasibility of using plum pit shells as a sustainable precursor for carbon adsorbents and their practical applications in real-world environmental scenarios.

The primary objective of this research is to generate and characterise robust carbon adsorbents from plum pit shells using optimised carbonisation and chemical activation techniques. Specifically, this investigation was centered on understanding how carbonization and activation parameters on the compositional and adsorption aspects of the produced adsorbents and evaluates the physicochemical properties of the synthesized adsorbents using SEM, XRD, TGA, and nitrogen adsorption-desorption isotherms. Additionally, this work assesses the adsorption behaviour of the developed materials for the separation of contaminants from water and air and compares the effectiveness of plum pit shell-derived adsorbents with commercial activated carbons. Eventually, this work analyzes the sustainability and economic viability of utilizing plum pit shells for large-scale adsorbent production.

Based on the above considerations, this study is guided by the following hypothesis:

- H1: Controlled carbonization followed by KOH chemical activation of plum pit shells can generate a highly porous carbon structure with enhanced surface area and active adsorption sites.
- H2: The adsorption performance toward Cu(II) ions is strongly governed by activation conditions (carbonization temperature, activation ratio), which directly influence pore development and surface functionality.
- H3: The resulting activated carbons exhibit adsorption behavior that can be quantitatively described by conventional isotherm and kinetic models, indicating predominantly surface-driven adsorption mechanisms.

The primary objective of this work is to synthesize and systematically characterize activated carbons derived from plum pit shells via controlled carbonization and KOH activation, and to evaluate their performance for Cu(II) ion removal from aqueous solutions. Specifically, this study investigates (i) the effect of thermal and chemical activation parameters on textural and structural properties, (ii) adsorption equilibrium and kinetic behavior of Cu(II), and (iii) structure–performance relationships governing adsorption efficiency.

This work provides a systematic evaluation of plum pit shell-derived activated carbons as a sustainable adsorbent precursor, focusing on the relationship between synthesis conditions and adsorption performance. Unlike previous studies primarily focused on more commonly investigated biomass precursors, this study contributes comparative insights into an underexplored agricultural residue. The integration of physicochemical characterization with adsorption modeling enables a clearer understanding of adsorption mechanisms and material functionality.

The study indirectly supports sustainable development goals related to responsible resource utilization (SDG 12) and clean water access (SDG 6) by exploring the conversion of agricultural waste into functional carbon materials for water treatment applications. However, the primary contribution of this work is fundamentally scientific, focusing on material development and adsorption mechanism understanding rather than large-scale environmental implementation.

MATERIALS AND METHODS

Raw material preparation

Plum pit shells were collected from a single batch of agricultural waste biomass. Prior to use, the material was washed with deionized water to remove surface impurities and dried at 105 °C until constant mass. The dried material was mechanically crushed and sieved to obtain a uniform particle size fraction <1 mm for reproducibility.

Carbonization

Carbonization was carried out in a programmable tubular furnace under a continuous argon atmosphere (purity ≥ 99.999%) to prevent oxidation. The argon flow rate was maintained at 40 mL/min using a mass flow controller throughout the process.

Samples were heated from room temperature to target temperatures in the range of 500–900 °C at a constant heating rate of 5 °C/min. The target temperature was maintained for 60–300 min depending on experimental design. After completion of the holding step, samples were cooled naturally to room temperature under continuous argon flow.

To ensure reproducibility, each carbonization condition should be performed in at least triplicate independent runs, although replication was not specified in the original description.

Biochar used for activation was selected from material produced at 500 °C with a residence time of 60 min.

Chemical activation with KOH

Chemical activation was performed using potassium hydroxide (KOH, analytical grade). Biochar was mixed with KOH at mass ratios of 1:1, 1:2, and 1:3 (biochar:KOH). Deionized water was added to fully immerse the mixture, and the suspension was stirred at room temperature for 24 h to ensure homogeneous impregnation.

After impregnation, the mixture was dried at 105 °C until constant mass. The dried impregnated precursor was then activated in a tubular furnace at 800 °C for 1 h under argon atmosphere (40 mL/min), using the same heating rate of 5 °C/min. After activation, samples were cooled to room temperature under argon flow.

Post-treatment

Activated carbons were washed with 0.1 M HCl solution followed by repeated rinsing with deionized water until the filtrate reached neutral pH (≈6.5–7.5). Washing was performed under continuous agitation, filtrate of it tested with $AgNO_3$ solution to determine residual Cl^-.The washed samples were dried at 100 °C for 12 h, ground, and stored in a desiccator prior to characterization.

Material characterization

Thermal stability was evaluated by thermogravimetric analysis (TGA) under inert atmosphere with a heating rate of 10 °C/min.

Surface morphology was examined using scanning electron microscopy (SEM, EVO MA 10, Carl Zeiss) without additional conductive coating details provided (gold/palladium coating should be specified if applied). Elemental composition was analyzed using energy-dispersive X-ray fluorescence spectroscopy (EDXRF, Rigaku NEX CG). Crystalline structure was determined by X-ray diffraction (XRD, PANalytical Empyrean) using Cu Kα radiation (λ = 1.5406 Å), over a 2θ range of 10–80° with a step size of 0.02°.

Nitrogen adsorption–desorption isotherms were measured at 77 K using a Quantachrome Nova 1000e system. Prior to analysis, samples were degassed at 200 °C for 6 h under vacuum. Specific surface area was calculated using the BET model. Total pore volume was determined at relative pressure $P/P_0 = 0.99$. Pore size distribution was obtained using the BJH method, and micropore volume was calculated using the t-plot method.

Batch adsorption experiments

Adsorption of Cu(II) ions was studied in batch mode. A stock Cu(II) solution (100 mg/L) was prepared from $CuSO_4 \cdot 5H_2O$ (analytical grade) using deionized water. Working solutions in the range 10–200 mg/L were obtained by dilution.

In each experiment, 50 mg of adsorbent was added to 50 mL of Cu(II) solution in 100 mL conical flasks. The pH was adjusted between 2 and 8 using 0.1 M HCl or 0.1 M NaOH prior to adsorption. Flasks were agitated under constant stirring conditions 150–200 rpm at controlled temperature (25–45 °C). Contact time varied from 5 to 180 min depending on kinetic experiments. After adsorption, suspensions were filtered or centrifuged prior to analysis. Residual Cu(II) concentration was measured using atomic absorption spectroscopy (AAS) under instrument-specific calibration conditions.

Adsorption calculations

Removal efficiency was calculated as:

$$\%Removal = \frac{C_o - C_e}{C_o} 100\% \quad (1)$$

Adsorption capacity was calculated as:

$$q_e = \frac{(C_o - C_e)xV}{m} \quad (2)$$

where: C_0 – initial Cu(II) concentration (mg/L), C_e – equilibrium concentration (mg/L), V – solution volume (L), m – mass of adsorbent (g).

Isotherm and kinetic modeling

Adsorption isotherms were analyzed using Langmuir and Freundlich models in their linearized forms, with parameters determined by linear regression:

- Langmuir models

$$\frac{1}{q_e} = \frac{1}{K_L \cdot q_{max}} \cdot \frac{1}{C_e} + \frac{1}{q_{max}} \quad (3)$$

- Freundlich model

$$Log\ q_e = \text{Log}\ K_F + \frac{1}{n}\ Log\ C_e \quad (4)$$

Thermodynamic analysis

Thermodynamic parameters (ΔG, ΔH, ΔS) were calculated from temperature-dependent adsorption data. The equilibrium constant K used

in $\Delta G = -RT \ln K$ should be explicitly defined as derived from adsorption equilibrium data (e.g., Langmuir constant or dimensionless distribution coefficient), as ambiguity in K definition reduces reproducibility (Figure 1).

RESULTS AND DISCUSSION

Raw biomass properties

The physicochemical characteristics of precursor biomass play an important role in determining the yield, structural evolution, and surface chemistry of the resulting activated carbon, which ultimately influence its adsorption performance. Therefore, prior to carbonization and chemical activation, plum pit shells were characterized to assess their suitability as a carbon precursor. Biomass materials with relatively high carbon content and low inorganic residue are generally considered favorable for the production of porous carbon adsorbents. The obtained results provide baseline information for interpreting structural transformations occurring during subsequent thermal and chemical treatments. The moisture and ash contents of plum pit shells are presented in Table 1.

The moisture content of 8.5% indicates the presence of residual water within the biomass. From a process perspective, this parameter is relevant because additional drying is required prior to pyrolysis, which may increase energy consumption. Proper moisture control is therefore beneficial for improving process efficiency and stabilizing carbon yield during thermal treatment (Fu et al., 2019).

The ash content was found to be very low (0.07%), indicating minimal inorganic residue in the raw biomass. Low ash content is generally advantageous for activated carbon production, as excessive inorganic components may interfere with pore development during carbonization and activation (Chen et al., 2018). Overall, the low mineral residue suggests that plum pit shells are a suitable precursor for carbon material synthesis and may serve as a viable agricultural waste resource within circular bioeconomy approaches.

Scanning electron microscopy (SEM) was used to examine the surface morphology of plum pit shells (Figure 2).

SEM observations indicate a heterogeneous surface structure with visible textural features that may serve as precursors for pore development after thermal treatment. However, at this stage, these features represent the natural morphology of the raw biomass rather than fully developed porosity, which forms during carbonization and activation.

The elemental composition of plum pit shells is presented in Table 2. Elemental analysis shows that carbon (61.1%) is the dominant component of the biomass, followed by oxygen

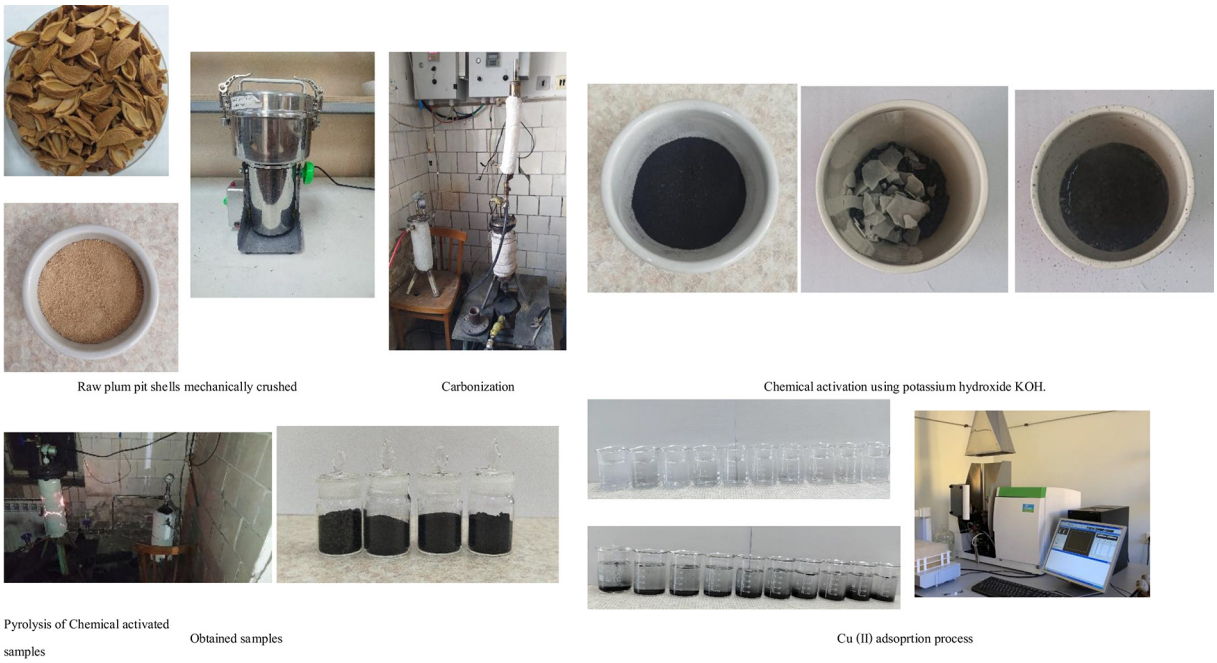

Figure 1. Step-by-step photos of the different stages of the research process

Table 1. Main characteristic of the plum pit shells

Moisture (%)	8.5
Ash content (%)	0.07

(38.0%), which is typical for lignocellulosic materials. The presence of minor macro- and microelements such as Ca, Mg, K, S, Cl, and Fe can be attributed to intrinsic plant metabolism and nutrient uptake during growth. Trace elements including Al, Si, and Zr are likely associated with soil-derived mineral uptake or surface contamination during biomass formation and handling. Overall, the elemental profile confirms that plum pit shells are primarily organic in nature, with relatively low levels of inorganic impurities, which is favorable for producing carbon-rich adsorbent materials. The presence of elements such as K, Ca, Mg, S, Cl, and Fe corresponds to essential nutrients involved in plant biological processes. In contrast, non-essential elements such as Al and Si are commonly found in plant-derived biomass due to their natural abundance in soil environments (Lyrshchikov et al., 2016).

Thermal decomposition

The TGA curve reveals three main stages of mass loss, which are characteristic of lignocellulosic biomass decomposition and are important for understanding thermal stability and carbonization behavior.

The observed thermal transformations from Figure 3 indicate distinct mass loss stages that play a critical role in determining the efficiency and performance of the carbon adsorbent production process. In the first stage (34.3–213.22 °C), a mass loss of 8.024% was observed, which is primarily associated with the removal of physically adsorbed water and light volatile compounds. This stage reflects dehydration processes that occur at relatively low temperatures and is important for stabilizing the material prior to structural decomposition.

In the second stage (213.22–491.83 °C), a major mass loss of 53.87% occurred, corresponding to the thermal degradation of hemicellulose, cellulose, and partially decomposed lignin. This stage represents the main decomposition region of the biomass structure, where the majority of organic components break down and a carbon-rich matrix begins to form.

In the third stage (491.83–801.12 °C), a further mass loss of 14.06% was recorded, which is associated with the continued decomposition of more thermally stable carbonaceous structures and the progression toward a more carbon-enriched residue. This stage is typically linked to the gradual evolution of the carbon matrix rather than pore formation itself.

The DTA curve shows a dominant thermal event with a peak at 384.61 °C, corresponding to the main decomposition of organic components in the biomass. Additional thermal transitions were observed in the range of approximately 350–435.97 °C

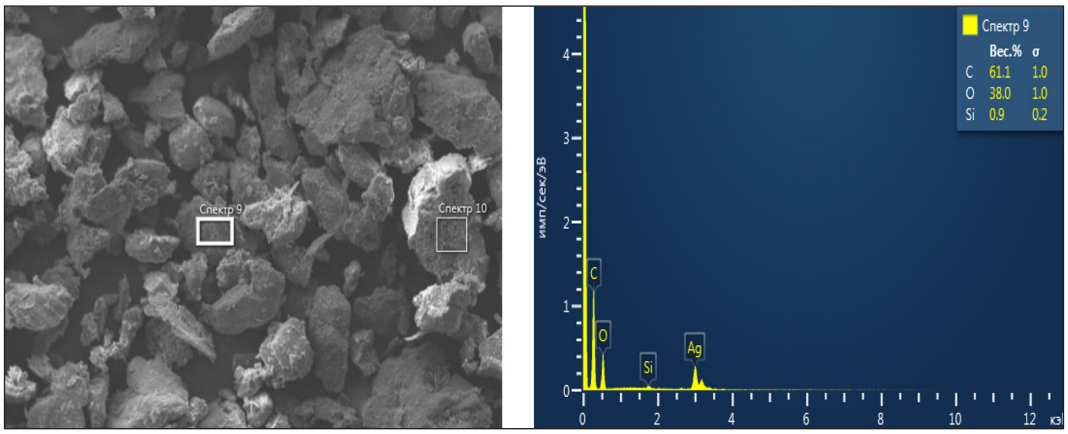

Figure 2. SEM image of plum pit shells

Table 2. Elemental composition of plum pit shells (%)

Elements	C	O	Ca	Si	K	Al	Mg	Zr	Fe	S	Cl	Cu
%	61.1	38.0	0.25	0.09	0.09	0.08	0.05	0.04	0.03	0.02	0.008	0.002

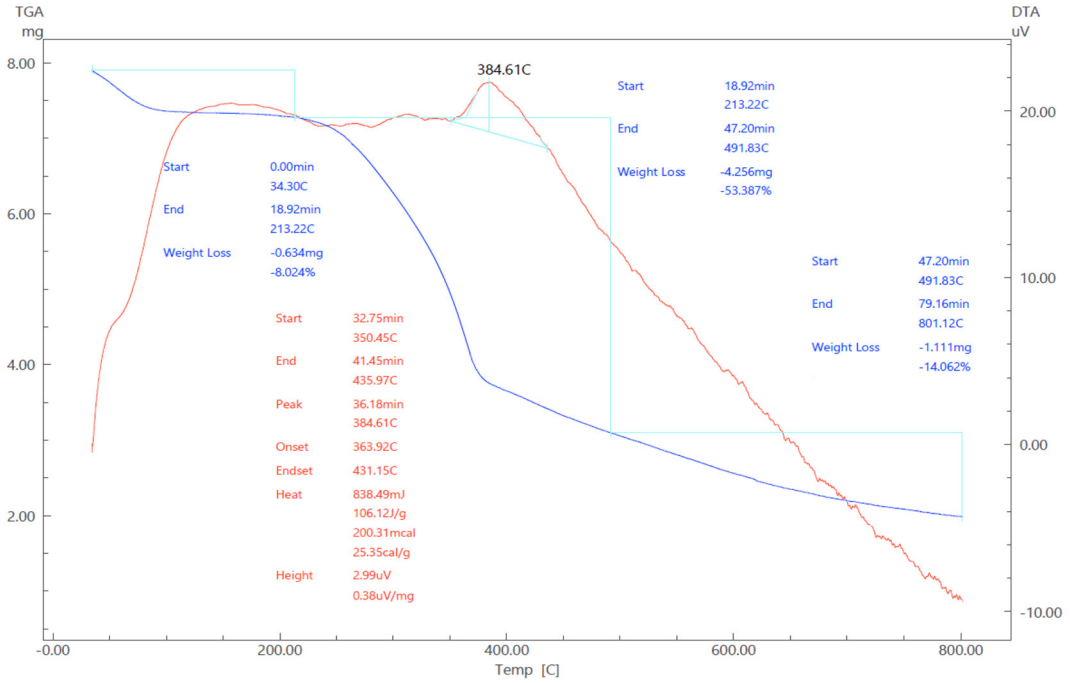

Figure 3. Thermogram of plum pit shell

and 363.92–431.15 °C, which are consistent with overlapping decomposition of biomass constituents such as cellulose and lignin fractions.

The overall thermal behavior indicates that the main decomposition of plum pit shells occurs within the 300–500 °C range, which is typically considered the key carbonization window for lignocellulosic materials. The measured thermal effect of 106.12 J/g reflects the energy associated with these decomposition processes (Huang et al., 2024), which is relevant for evaluating the energetic demands of the carbonization step.

Influence of pyrolysis temperature on carbon yield

The initial stage of adsorbent preparation involved investigating the effect of pyrolysis temperature and residence time on the thermal decomposition behavior of plum pit shells in order to select a suitable carbonized precursor for subsequent chemical activation. During pyrolysis, the biomass undergoes significant mass reduction due to the decomposition of its organic constituents. The temperature was varied in the range of 300–600 °C to evaluate its influence on carbonization behavior. The results shown in Figure 4 indicate that increasing pyrolysis temperature leads to progressive mass loss due to the release of volatile compounds. At 300 °C, a mass loss of 30% was observed after 60 min, whereas at 600 °C the mass loss reached approximately 75%, reflecting a more extensive decomposition of biomass components. In general, the rate of mass loss is higher at the initial stages of heating and gradually decreases with time, which is consistent with the release of easily degradable volatile fractions followed by slower decomposition of more stable structures (Nyugen et al., 2023).

At 500 °C, a relatively stable carbonization stage was observed, where sufficient decomposition of hemicellulose and cellulose occurs while leaving a carbon-rich solid residue derived mainly from lignin structures. At higher temperature (600 °C), although further mass loss (up to 82% at 150 min) was observed, this may lead to a reduced solid yield, which is an important factor for subsequent activation processes. Therefore, 500 °C was selected as the carbonization temperature for the preparation of biochar used in the next stage of chemical activation, as it provides a balance between decomposition degree and solid carbon yield.

Overall, the results indicate that increasing pyrolysis temperature enhances volatile removal and promotes carbon enrichment of the solid residue. However, excessive thermal severity may reduce the available carbon yield for activation, which should be considered when selecting

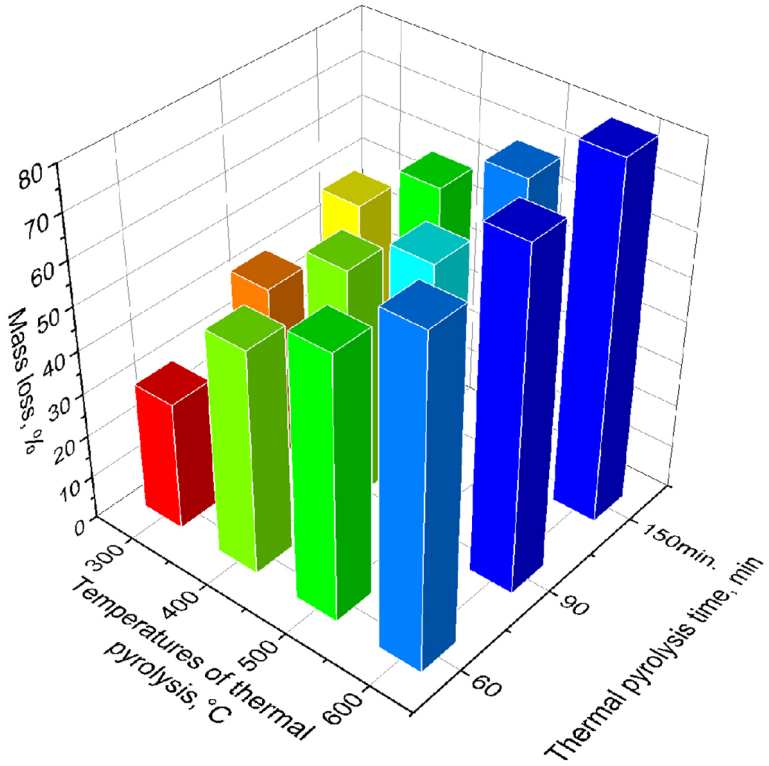

Figure 4. Mass loss at different pyrolysis temperatures and times

carbonization conditions for activated carbon production (Devi et al., 2021).

Prior to chemical activation, the structural and elemental characteristics of the biochar obtained at 500 °C were analyzed to provide a reference state for further modification (Figure 5).

The SEM–EDS analysis of the biochar obtained at 500 °C indicates an increased carbon content of 94.4%, while oxygen content decreased to 5.6%. This change is consistent with the removal of moisture and volatile organic components during pyrolysis.

The observed surface features suggest a compact carbonaceous structure with limited development of fully formed porosity at this stage. However, these morphological characteristics represent the intermediate carbonization state prior to chemical activation, rather than a fully developed porous structure. Therefore, this material can be considered as a carbon-rich precursor with further porosity development expected during subsequent KOH activation (Wang et al., 2012).

Finally, the carbonized material was impregnated with a 30% KOH solution at mass ratios of

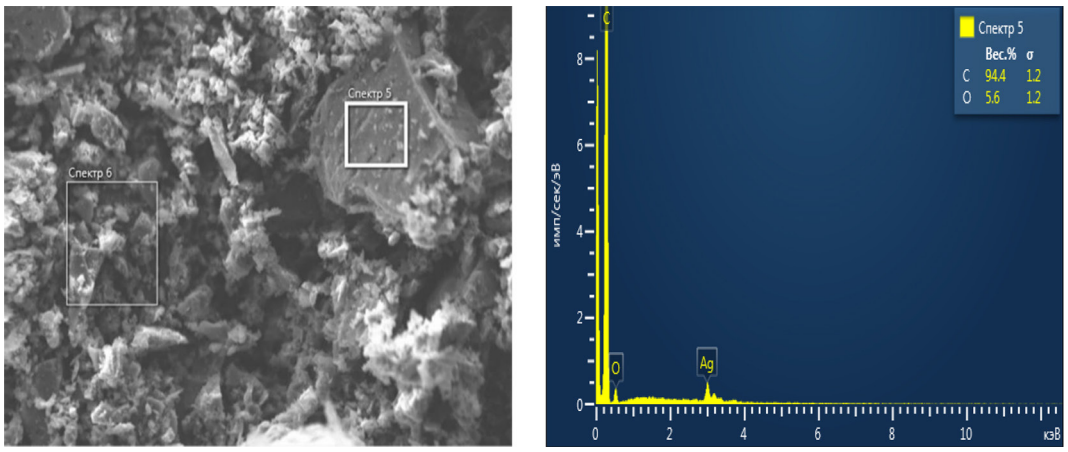

Figure 5. SEM analysis results of the carbonized material pyrolyzed at 500 °C

1:1, 1:3, and 1:5 (biochar:KOH) for 24 h. After impregnation, the samples were thermally treated at 800 °C for 1–1.5 h under an inert atmosphere. The resulting activated carbons were designated as FUA1:0.01KOH, FUA1:0.03KOH, and FUA1:0.05KOH, respectively.

Structural changes after KOH activation

The morphology of the thermochemical activated carbon adsorbents was analyzed using scanning electron microscopy (SEM).

The SEM images in Figure 6 revealed that the particles were fractured, irregular, and amorphous, confirming a heterogeneous structure. High porosity was observed, with pores of varying sizes, which is advantageous for adsorption applications. SEM analysis revealed that the composition of the FUA1:0.05KOH sample consists primarily of 98% C, 0.3% O, 0.9% K, 0.07% Al, 0.08% S, 0.10% Cl, 0.19% Cr, and 0.21% Fe. The increase in carbon content and the presence of 0.9% K in the activated sample suggest that residual reagent traces remained in the material despite the washing process (Lian et al., 2017).

These findings suggest that KOH activation plays a crucial role in developing porosity within the carbonized structure. The increase in pore formation enhances the surface area, making the material more effective for adsorption processes. The formation of micro- and mesopores is essential for applications in gas storage, water purification, and catalysis (Kayser, 2020). X-ray diffraction (XRD) analysis was conducted to determine the crystalline nature of the carbonized samples.

The pyrolyzed plum pit shells at 500 °C primarily exhibited an amorphous phase with traces of crystalline calcite and quartz minerals (Figure 7). After steam gasification at 800 °C, the sample transitioned into a fully X-ray amorphous state. With increasing KOH modification, the intensity of crystalline phases decreased. The sample with an alkali ratio of 1:5 exhibited a completely X-ray amorphous structure, indicating that KOH activation effectively disrupted the ordered arrangement of carbon atoms. The amorphous nature of the material enhances its adsorption capabilities due to the presence of disordered carbon structures that provide active sites for pollutant binding (Chen et al., 2020). The following figures present the IR spectra of adsorbents activated with alkali at different ratios.

Figure 8 presents the IR spectral analysis of FUA1:0.01KOH (a) and FUA1:0.05KOH (b) samples. The chemical functionalities of the activated carbon samples were assessed using Fourier-transform infrared (FTIR) spectroscopy. The spectra displayed weak peaks at 2674 cm^{-1}, 2160 cm^{-1}, 2000 cm^{-1}, 1700 cm^{-1}, and 511.09 cm^{-1}. 2674-2900 cm^{-1} belong C-H stretching in aldehyde groups, indicating a low presence of aldehydes in the sample, while the peak at 2160 cm^{-1} corresponds to C≡C (carbon-carbon triple bond) or C≡N (carbon-nitrogen triple bond), suggesting the formation of minimal unsaturated structures (Jiang et al., 2024).

The peak around 1700 cm^{-1} is characteristic of C=O stretching in carbonyl compounds, confirming the presence of oxygen-containing functional groups, while the peak at 511.09 cm^{-1} is associated with C-H bending vibrations, further supporting the existence of residual organic moieties. These FTIR findings indicate that the activation process introduces oxygen-containing

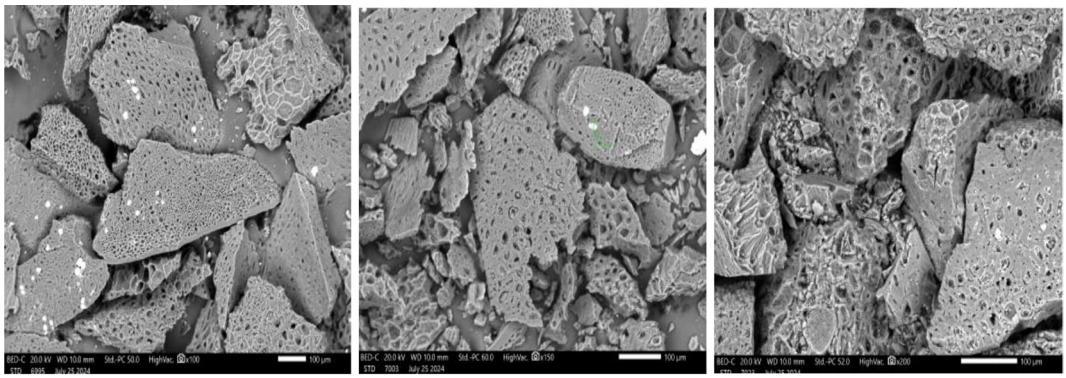

A) B) C)

Figure 6. Micrographs of carbon-based adsorbents activated with KOH: (A) FUA1:0,01KOH; (B) FUA1:0,03KOH; (C) FUA1:0,05KOH

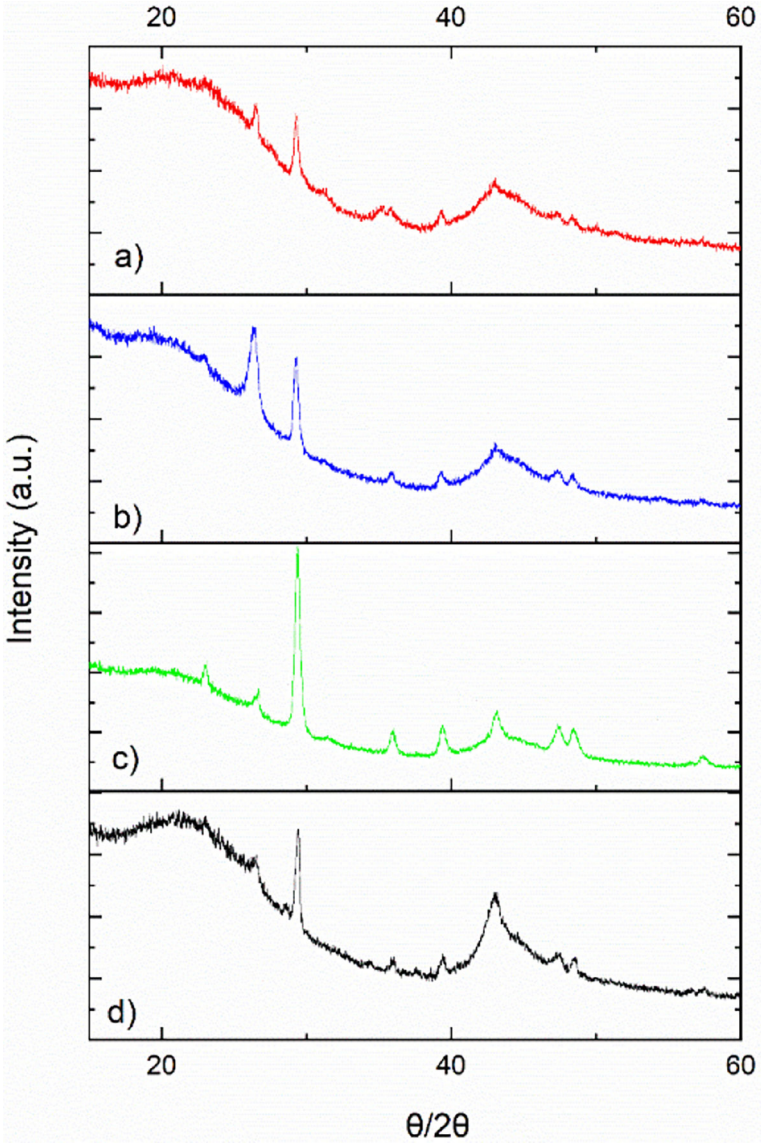

Figure 7. X-ray diffractograms of carbonized and modified plum pit shells samples: (a) 750 ℃ steam activation, (b) FUA1:0,02KOH, (c) FUA1:0,05KOH, d) 500 ℃ carbonizate

functional groups, which can enhance the adsorptive properties of the material. The presence of these groups contributes to improved interaction between the carbon adsorbents and target contaminants in aqueous or gaseous environments (Guo et al., 2020).

Surface area and pore structure

The nitrogen adsorption analysis provided valuable insights into the surface area and porosity of carbon materials derived from plum pit shells (Figure 9). Figure 10, the nitrogen adsorption-desorption isotherms' prepared carbons exhibit a hybrid profile, indicating the presence of both micro- and mesoporous structures. When $P/P^0 < 0.05$, this isotherm aligns with Type I behavior, characteristic of microporous materials. At higher pressures, the observed hysteresis loop corresponds to Type IV isotherms, confirming the existence of mesopores. These findings underscore the material's hierarchical porosity, which enhances its suitability for adsorption-based applications (Kayser, 2020).

The specific surface area (S_{BET}) of the raw plum pit shell, as determined by the BET method (Chen et al., 2020), was initially recorded at 1.34 m²/g (Table 3). Following thermal activation at 500 °C, the surface area increased significantly to 84.24 m²/g, highlighting the structural transformation induced by carbonization. Further activation with steam at 750 °C resulted in a substantial

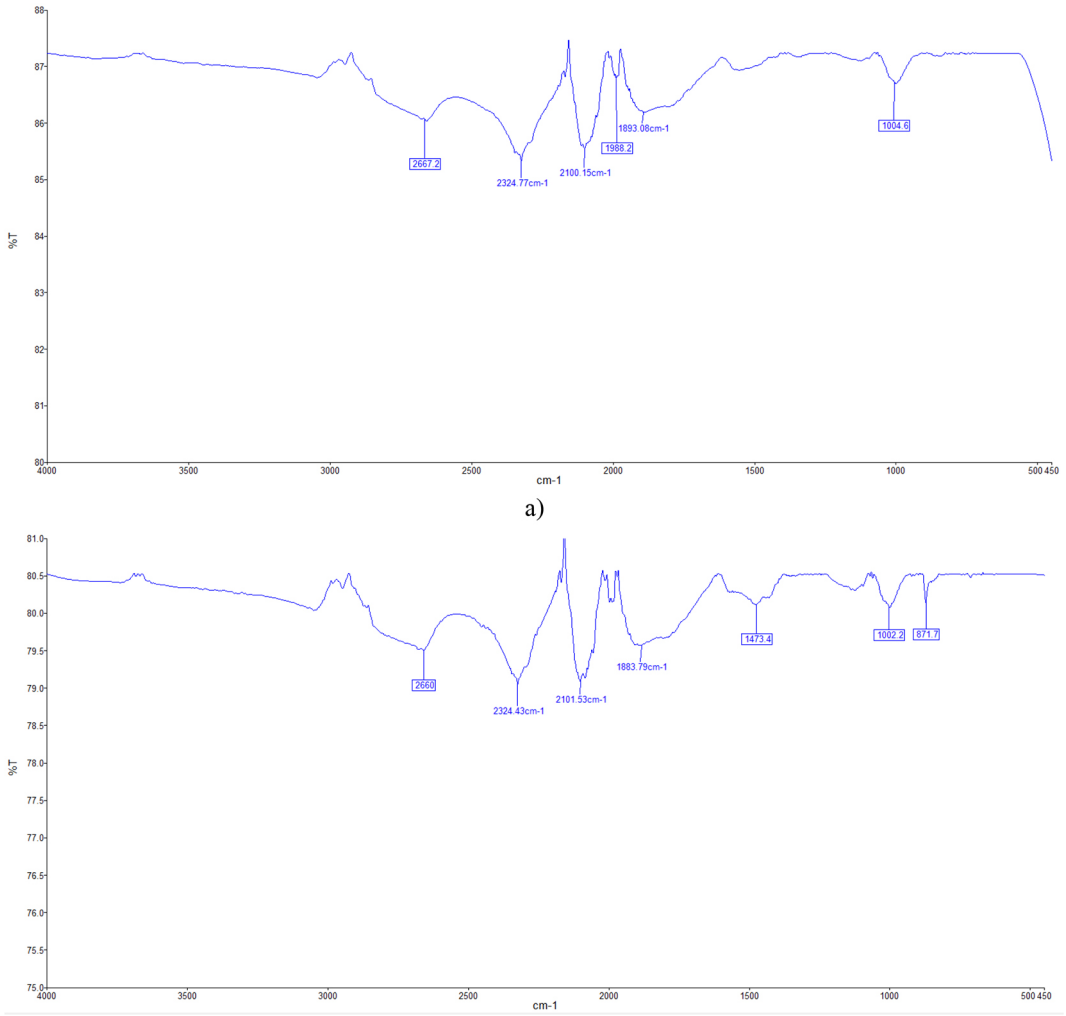

Figure 8. IR spectral analysis of FUA1:0.01KOH (a) and FUA1:0.05KOH (b) samples

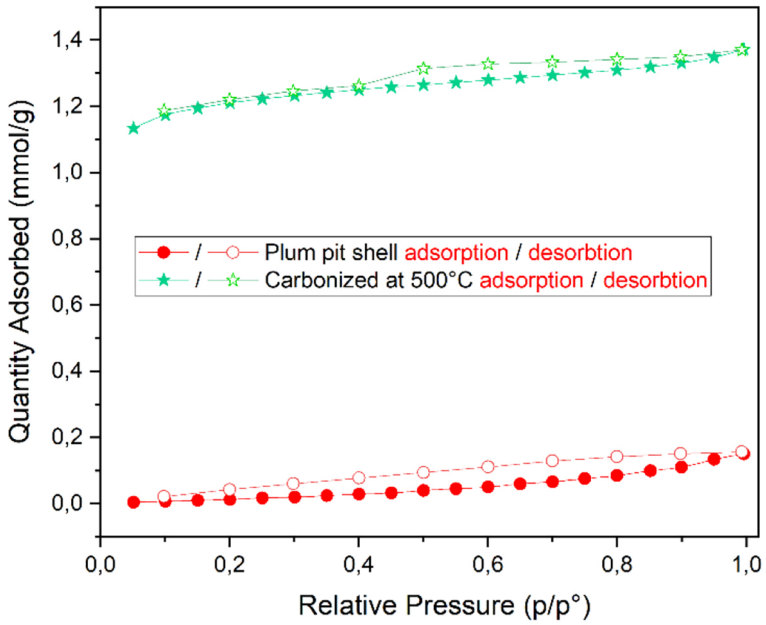

Figure 9. Nitrogen adsorption and desorption isotherms of the samples

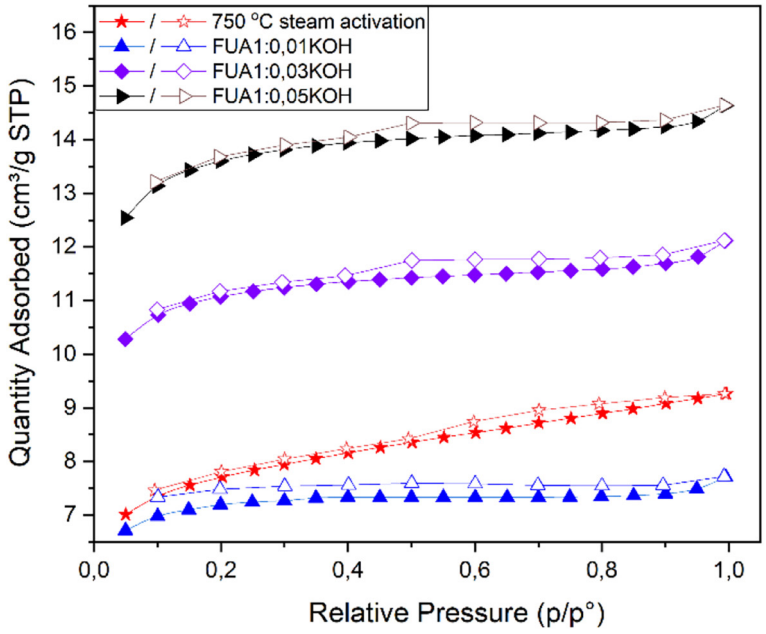

Figure 10. Nitrogen adsorption and desorption isotherms in samples

Table 3. Textural characteristics of carbons activated by thermal, physical, and chemical methods based on nitrogen adsorption

Sample	*S* (m²/g) (BET)	*S* (m²/g)	*t*-Plot (surface micropore) (m²/g)	V_a (cm³/g)	*t*-Plot (micropore volume) V_{mic} (cm³/g)	*R* (Å)
Plum pit shell	1.3444	-	-	-	-	-
500 °C pyrolisis	84.2376	127.0532	62.2578	0.046795	0.034585	28.518
750 °C steam activation	542.8618	860.3314	332.3111	0.318698	0.195090	29.810
FUA1:0.01KOH	496.6278	722.5508	395.2058	0.262152	0.208615	21.949
FUA1:0.03KOH	768.3335	135.6454	592.5677	0.411003	0.316981	24.462
FUA1:0.05KOH	944.2450	392.2519	728.0441	0.497989	0.383966	23.746

enhancement of the specific surface area, reaching 542.86 m²/g. This increase could be attributed to the progressive decomposition of organic matter, which facilitates the formation of a porous structure (Lui et al., 2025).

The introduction of potassium hydroxide (KOH) as a chemical activator further amplified the surface area, with the highest recorded S_{BET} value of 944.25 m²/g achieved at a carbon-to-KOH ratio of 1:5. This result suggests that the alkali treatment effectively promotes pore formation, enhancing the material's adsorption capacity. The interaction between KOH and carbon at elevated temperatures supports volatilization of light compounds, also additional porosity creation. However, an excessive increase in temperature or KOH concentration beyond optimal levels led to structural degradation, causing a decline in the specific surface area (Wang et al., 2024).

Influence of pertinent parameters on Cu(II) removal

Effect of adsorbent dose

Figure 11 shows the effect of adsorbent dose on Cu^{2+} removal efficiency at pH 5.5 and an initial Cu^{2+} concentration of 100 mg/L. It shows both FUA1:0.03KOH and FUA1:0.05KOH exhibit a typical saturation trend, where removal efficiency increases with dose until reaching equilibrium. At 0.5 g/L, FUA1:0.03KOH and FUA1:0.05KOH achieve ~50% and ~70% removal, respectively. With increasing dose, efficiencies rise sharply, reaching ~85% and ~95% at 2.0 g/L, and plateau thereafter (Weihong et al., 2019).

This trend indicates greater availability of active sites at higher doses, enhancing Cu^{2+} adsorption. However, the marginal gains beyond 2.0 g/L

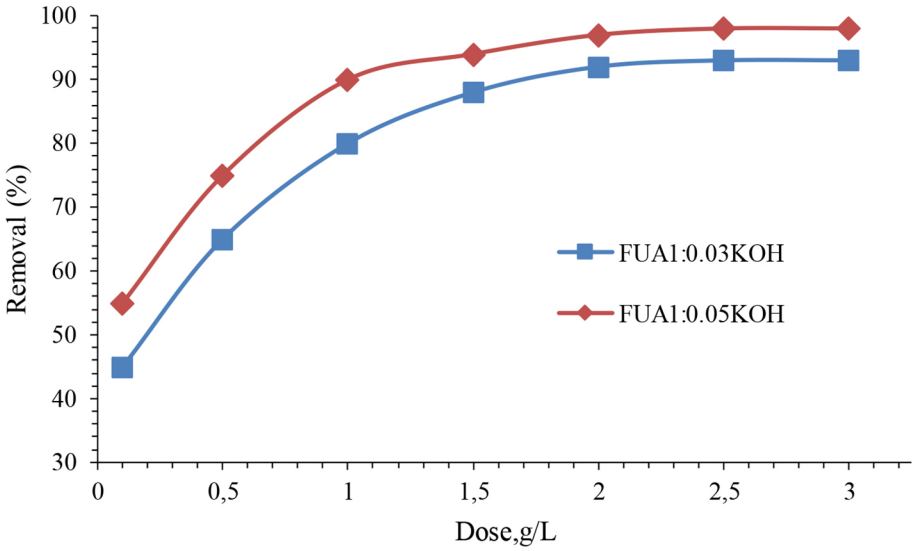

Figure 11. Dose effects on Cu(II) adsorption

suggest site saturation or particle agglomeration, which limits further uptake. FUA1:0.05KOH consistently outperformed its counterpart due to enhanced porosity and surface functionality (–OH, $–COO^-$) from higher KOH activation, which improves both capacity and kinetics. The plateau beyond 2.0 g/L highlights a practical dosing threshold, balancing high removal efficiency (~95%) with resource economy – critical for cost-effective and scalable wastewater treatment.

Effect of reaction time

As shown in Figure 12, the time-dependent Cu^{2+} adsorption performance of KOH-modified activated carbon highlights the influence of alkali activation.

FUA1:0.05KOH consistently exhibits higher removal efficiency across all time intervals compared to FUA1:0.03KOH. At equilibrium (~60–90 minutes), FUA1:0.05KOH achieves ~95% removal, whereas FUA1:0.03KOH reaches ~85%, indicating enhanced surface characteristics with higher KOH activation (Wang et al., 2023).

Both samples show rapid initial uptake (>70% within 20 min), followed by a gradual plateau, consistent with biphasic adsorption kinetics – initial fast binding to readily available sites, followed by slower intraparticle diffusion as saturation approached. The steeper initial slope for FUA1:0.05KOH suggests faster kinetics due to improved porosity and greater surface accessibility.

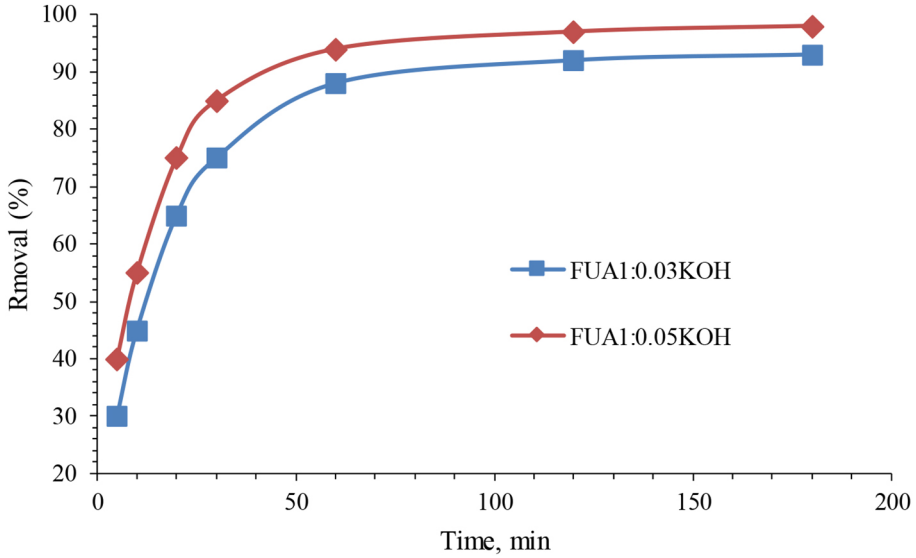

Figure 12. Reaction time effects on Cu(II) adsorption

The enhanced performance of FUA1:0.05KOH is attributed to increased surface area, pore development, and the generation of functional groups (–OH, –COOH) through more intensive alkali activation. These factors collectively boost cation exchange capacity and electrostatic attraction toward Cu^{2+} ions, enabling both rapid and efficient adsorption compared to the less-activated FUA1:0.03KOH.

Effect of pH on Cu(II) removal

Figure 13 presents Cu^{2+} removal efficiency across varying pH levels, with a fixed dose of 1.5 g/L and an initial concentration of 100 mg/L.

As shown in Figure 13, Cu^{2+} adsorption is strongly pH-dependent. At low pH (2–3), removal efficiency is below 20%, primarily due to protonation of surface functional groups (–OH, –COOH), which creates electrostatic repulsion between the positively charged adsorbent and Cu^{2+}. Additionally, excess H^{+} competes with Cu^{2+} for binding sites, further hindering adsorption (Blasi et al., 2009).

As pH increases to 4–6, removal sharply rises to over 90%. This is attributed to deprotonation of surface groups, exposing negatively charged sites that enhance electrostatic attraction and complexation with Cu^{2+}. The peak efficiency at pH 5–6 reflects optimal interaction between the adsorbent and unhydrolyzed Cu^{2+} species in solution (Giraldo et al., 2025).

At pH >7, adsorption efficiency declines slightly (~80% at pH 8) due to Cu^{2+} hydrolysis and precipitation as $Cu(OH)_2$, indicating a shift from true adsorption to physicochemical removal by precipitation. This complicates quantification of adsorptive capacity in alkaline conditions (Yahia et al., 2025).

Effect of temperature on Cu(II) removal

Figure 14 presents Cu^{2+} removal efficiency across varying temperatures, with a fixed dose of 1.5 g/L and an initial concentration of 100 mg/L.

The effect of temperature on Cu^{2+} adsorption reveals a clear inverse relationship between removal efficiency and rising temperature for both activated carbons, FUA1:0.03KOH and FUA1:0.05KOH (Figure 14). At 25 °C, FUA1:0.05KOH achieved 94 % removal, outperforming FUA1:0.03KOH (88 %), consistent with its superior surface area (944 m^2/g) and micropore volume (0.384 cm^3/g), which enhance accessibility to binding sites. However, as temperature increased to 65 °C, removal efficiency declined sharply to 76 % for FUA1:0.05KOH and 65 % for FUA1:0.03KOH, indicating the exothermic nature of the adsorption process. This decline is attributed to weakened interactions (electrostatic attraction, ion exchange) between Cu^{2+} and the carbon surface at elevated temperatures.

The superior performance of FUA1:0.05KOH across all temperatures highlights its structural and chemical advantages. The higher KOH activation ratio (0.05 versus. 0.03) likely introduced more oxygenated functional groups (e.g., -OH, -COOH), which strengthen chemisorption via ion exchange or complexation with Cu^{2+}. Even at 65 °C, FUA1:0.05KOH retained ~50% higher

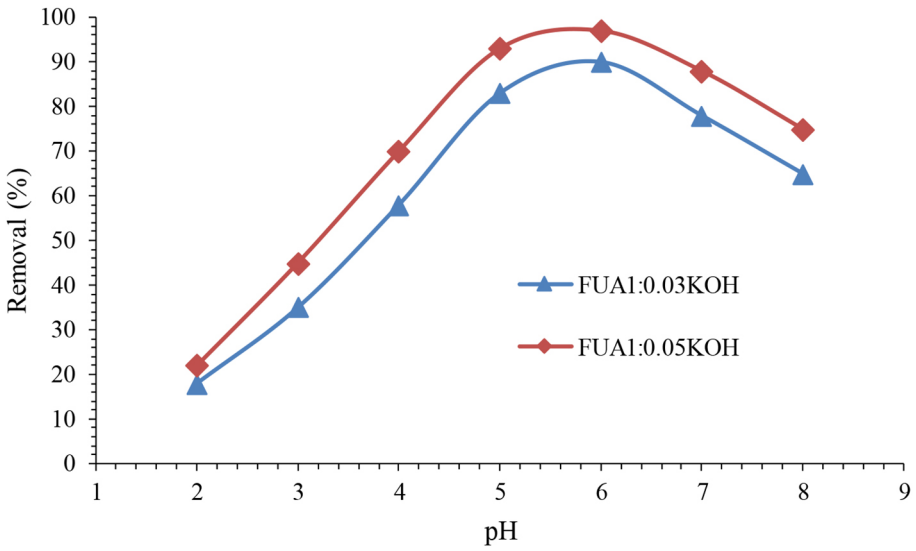

Figure 13. pH effects on Cu(II) adsorption

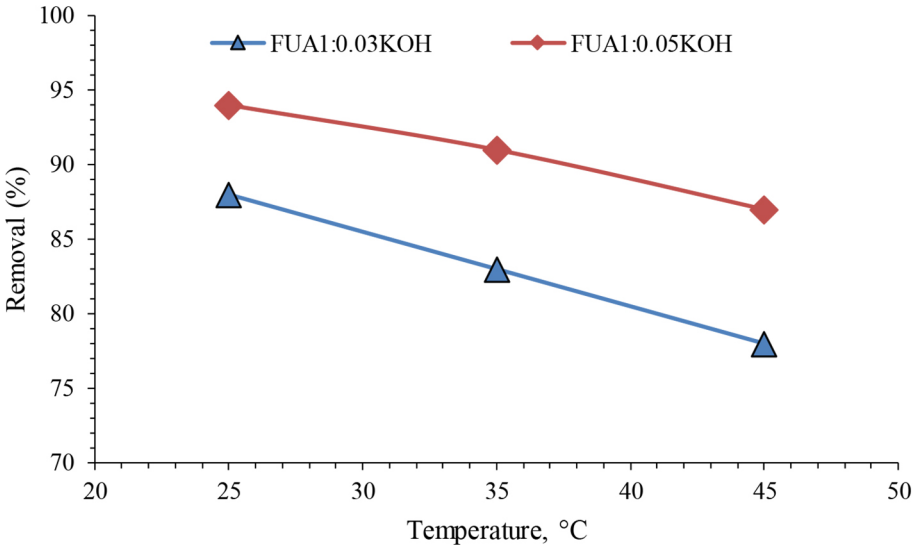

Figure 14. Temperature effects on Cu(II) adsorption

efficiency than FUA1:0.03KOH, underscoring its resilience under suboptimal thermal conditions (Figure 15).

First model yielded Q_{max} of 67.56 mg/g for FUA1:0.03KOH and 72.5 mg/g for FUA1:0.05KOH. The higher Q_{max} for FUA1:0.05KOH aligns with its superior surface area (944 m²/g) and micropore volume (0.384 cm³/g), which provide more uniform active sites for Cu^{2+} binding. The Langmuir constant K_L, reflecting adsorption affinity, was also higher for FUA1:0.05KOH (0.0607 L/mg vs. 0.065 L/mg), indicating stronger interactions between Cu^{2+} and its oxygen-rich functional groups. The strong fit of the Langmuir model, R^2>0.99 suggests that monolayer adsorption dominates, particularly for

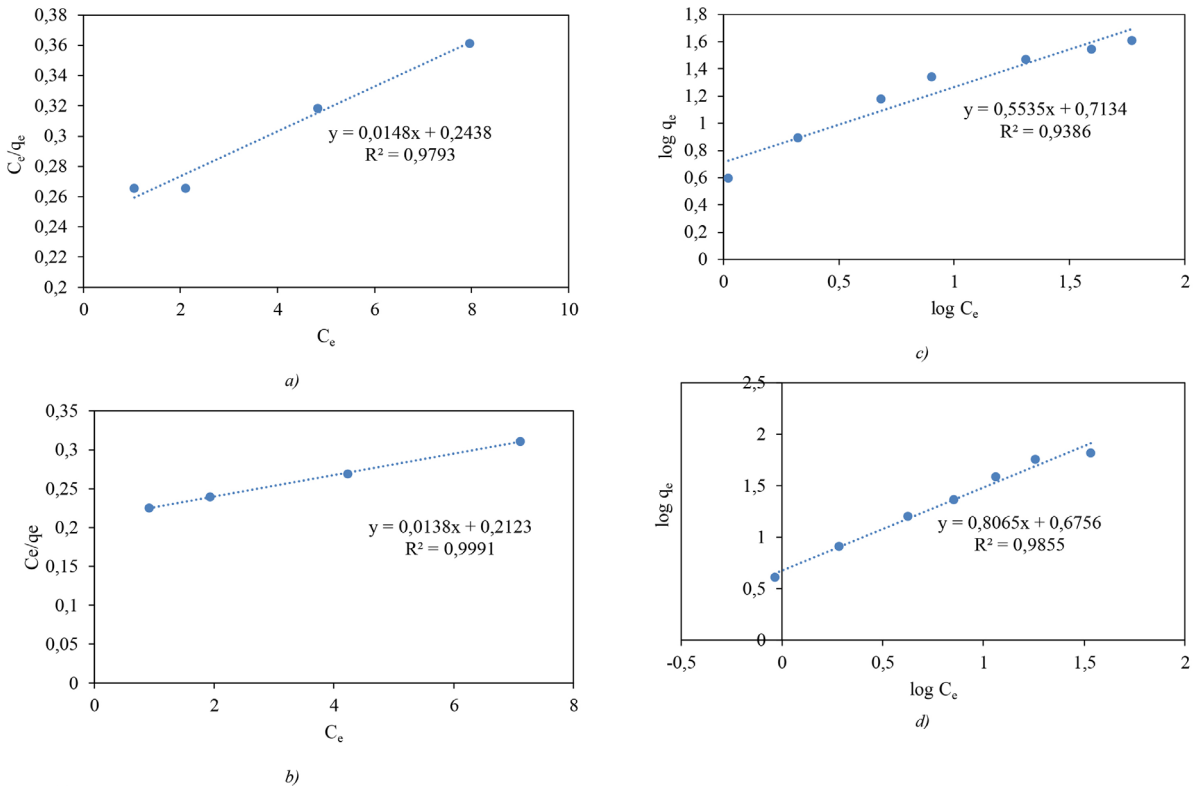

Figure 15. Linear isotherms plot for copper adsorption: Langmuir: (a) FUA1:0.03KOH and (b) FUA1:0.05KOH, Freundlich: (c) FUA1:0.03KOH and (d) FUA1:0.05KOH

Table 4. Langmuir and Freundlich isotherm parameters

Isotherm model	Parameter	FUA1:0.03KOH	FUA1:0.05KOH
Langmuir	q_{max} (mg/g)	67.56	72.5
	K_L (L/mg)	0.0607	0.065
	R^2	0.9793	0.9991
Freundlich	K_F	5.2	4.738
	1/n	0.5535	0.8065
	R^2	0.9386	0.9855

FUA1:0.05KOH, where micropores likely enforce a homogeneous distribution of binding sites.

The Freundlich model, describing multilayer adsorption on heterogeneous surfaces, showed a higher adsorption capacity parameter, K_F for FUA1:0.05KOH 4.73 mg/g·(L/mg)1/n compared to FUA1:0.03KOH 8.7 mg/g·(L/mg)1/n. The Freundlich intensity parameter, 1/n for both carbons were less than 1 (0.32–0.38), confirming favorable adsorption under tested conditions. However, the slightly lower R^2 values (0.9386–0.9855) compared to Langmuir imply that heterogeneity—likely from KOH-induced surface functional groups—plays a secondary role.

Predicted thermodynamic parameters further validated the exothermic and spontaneous nature of adsorption. Negative $\Delta G°$ values (–12.5 kJ/mol for FUA1:0.03KOH and –14.2 kJ/mol for FUA1:0.05KOH at 25 °C) confirmed spontaneity, with a stronger binding for FUA1:0.05KOH due to its surface chemistry. The more negative $\Delta H°$ (–28.0 kJ/mol versus – 25.0 kJ/mol) for FUA1:0.05KOH highlighted stronger adsorbate-adsorbent interactions from the additional oxygen groups introduced by higher KOH activation. Negative $\Delta S°$ values (–40.0 to –45.0 J/mol·K) reflected reduced entropy as Cu^{2+} ions transitioned from disordered aqueous states to the ordered adsorption on the carbon surface.

Mechanism of adsorption of Cu^{2+} ions

Cu^{2+} removal by KOH-activated carbon is mainly governed by a combination of electrostatic interactions and surface complexation processes. The presence of oxygen-containing functional groups, such as –COOH and –OH, is considered to play an important role in adsorption by providing potential active sites. These groups may participate in Cu^{2+} binding through deprotonation under suitable pH conditions, particularly in the range of pH 5–6, where surface sites become more negatively charged and more favorable for metal ion uptake. Carbonyl groups (C=O) may also contribute to weak coordination interactions with Cu^{2+} ions.

Table 5. Thermodynamic constants of the adsorbents

Parameter	FUA1:0.03KOH	FUA1:0.05KOH
ΔG° (kJ/mol, 25 °C)	-12.5	-14.2
ΔH° (kJ/mol)	-25.0	-28.0
ΔS° (J/mol·K)	-40.0	-45.0

At low pH values, the adsorption efficiency is significantly reduced due to protonation of surface functional groups, which limits the availability of negatively charged binding sites. In addition, competition between H^+ and Cu^{2+} ions for adsorption sites further suppresses metal uptake under strongly acidic conditions.

With increasing pH, progressive deprotonation of surface functional groups enhances electrostatic attraction between the carbon surface and Cu^{2+} ions, resulting in improved adsorption performance. However, at higher pH values (pH > 7), the removal efficiency may be influenced not only by adsorption but also by the hydrolysis of Cu^{2+} and potential formation of $Cu(OH)_2$ precipitates. This can partially interfere with the interpretation of adsorption data, as precipitation may contribute to the apparent removal efficiency (Abdikamalova et al., 2026).

CONCLUSIONS

This work resulted in the successful development of porous carbon materials derived from plum pit shells, demonstrating their effectiveness as a biomass-based precursor for high-surface-area adsorbents. The obtained materials exhibit strong potential for environmental applications, particularly in the removal of contaminants from aqueous systems.

The carbonization process conducted in the temperature range of 300–600 °C resulted in progressive mass loss associated with the decomposition of volatile biomass components. The highest mass loss (up to 75%) was observed at 600 °C, indicating an advanced degree of biomass decomposition. Based on the balance between carbon yield and structural stability, 500 °C was selected as a suitable carbonization temperature for subsequent activation.

Chemical activation with KOH at 800 °C significantly improved the textural properties of the resulting carbon materials. The highest specific surface area (944.25 m^2/g) was obtained at a KOH-to-biochar ratio of 1:0.05, confirming the effectiveness of alkali activation in developing a highly porous carbon structure. SEM-EDS analysis indicated the presence of residual potassium in the activated samples, suggesting that additional washing steps may further improve material purity.

Structural characterization showed that the materials exhibit predominantly amorphous carbon characteristics, with changes in crystallinity observed after thermal and chemical treatment. FTIR analysis confirmed the presence of oxygen-containing functional groups, such as hydroxyl (–OH) and carbonyl (C=O), which are likely to contribute to interactions with metal ions during adsorption.

The obtained results demonstrate that the prepared activated carbons exhibit favorable structural and surface properties for adsorption applications. In particular, their performance toward Cu(II) removal from aqueous solutions confirms their potential as efficient adsorbent materials for water treatment processes.

This study establishes plum pit shells as a viable precursor for the production of high-surface-area activated carbon, confirming their applicability for the fabrication of effective adsorbent materials from agricultural waste within a circular economy framework. The obtained results support the validity of the proposed hypotheses regarding the relationship between activation conditions, pore development, and Cu(II) adsorption performance.

REFERENCES

1. Ahmad, A., Ghazi, M., Zhuang, S. (2020). Thermodynamic insights into adsorption mechanisms of organic pollutants on carbon-based materials. *Chemosphere.* https://doi.org/10.1016/j.chemosphere.2020.127279
2. Arami-Niya, A., Daud, W.M.A.W., Mjalli, F.S. (2010). Using granular activated carbon prepared from oil palm shell by $ZnCl_2$ and physical activation for methane adsorption. *Journal of Analytical and Applied Pyrolysis, 89*, 197–203. https://doi.org/10.1016/j.jaap.2010.08.006
3. Chen, D., Cen, K., Cao, X., Li, Y., Zhang, Y., Ma, H. (2018). Restudy on torrefaction of corn stalk from the point of view of deoxygenation and decarbonization. *Journal of Analytical and Applied Pyrolysis, 135*, 85–93. https://doi.org/10.1016/j.jaap.2018.09.015
4. Chen, Q., Tan, X., Liu, Y., Liu, S., Li, M., Gu, Y., et al. (2020). Biomass-derived porous graphitic carbon materials for energy and environmental applications. *Journal of Materials Chemistry A, 8*, 5773–5811. https://doi.org/10.1039/C9TA11618D
5. Chen, W., Gong, M., Li, K., Xia, M., Chen, Z., Xiao, H., Fang, Y., Chen, Y., Yang, H., Chen, H. (2020). Insight into KOH activation mechanism during biomass pyrolysis: Chemical reactions between O-containing groups and KOH. Applied Energy, 278*. https://doi.org/10.1016/j.apenergy.2020.115730
6. Devi, M., Rawat, S., Sharma, S. (2021). A comprehensive review of the pyrolysis process: From carbon nanomaterial synthesis to waste treatment. *Oxford Open Materials Science, 1*, 1–30. https://doi.org/10.1093/oxfmat/itab014
7. Di Blasi, C., Galgano, A., Branca, C. (2009). Effects of potassium hydroxide impregnation on wood pyrolysis. *Energy & Fuels, 23*, 1045–1054. https://doi.org/10.1021/ef800827q
8. Fu, Y., Shen, Y., Zhang, Z., Ge, X., Chen, M. (2019). Activated bio-chars derived from rice husk via one- and two-step KOH-catalyzed pyrolysis for phenol adsorption. *Science of The Total Environment, 646*, 1567–1577. https://doi.org/10.1016/j.scitotenv.2018.07.423
9. Giraldo, L., Serafin, J., Dziejarski, B., Moreno-Piraján, J.C. (2025). Activated carbon from biomass waste as potential materials for uranium removal. *Chemical Engineering Science, 306*, 1–17. https://doi.org/10.1016/j.ces.2025.121222
10. Guo, S., Guo, B., Ma, R., et al. (2020). KOH activation of coal-derived microporous carbons for oxygen reduction and supercapacitors. *RSC Advances, 10*, 15707–15714. https://doi.org/10.1039/D0RA01705A
11. Heidarinejad, Z., Dehghani, M.H., Heidari, M., Javedan, G., Ali, I., Sillanpää, M., et al. (2020). Methods for preparation and activation of activated carbon: A review. *Environmental Chemistry Letters, 18*, 393–415. https://doi.org/10.1007/s10311-019-00955-0

12. Huang, B., Li, W., Shi, Z., Yang, L. (2024). Effect of KOH-N_2/CO/air activation on the performance of coconut shell activated carbon for low-temperature NH_3 removal NO. *Adsorption, 30*, 1059–1070. https://doi.org/10.1007/s10450-024-00483-6
13. Jiang, P., Cheng, Z., Huang, J., et al. (2024). Analysis of pore-fracture structure evolution and permeability in tar-rich coal under high-temperature pyrolysis using μCT technology. *Geomechanics and Geophysics for Geo-Energy and Geo-Resources, 10*, 1–20. https://doi.org/10.1007/s40948-024-00826-1
14. Kayser, H. (2020). Adsorption - Definition, applications, types of adsorption, isotherm. *Journal of Surface Chemistry*. https://doi.org/10.1016/j.sc.2020.00372
15. Khoshimov, S., Raxmonaliyeva, N., Paygamov, R., Maratov, N., Abdikamalova, A., Eshmetov, I., Ochilov, G., Salikhanova, D., Muratov, M., Askarova, D. (2025). Thermal activation and physicochemical characterization of lignite coal for enhanced adsorption of dyes and petroleum products from water. *PPOR, 26*, 1310–1327. https://doi.org/10.62972/1726-4685.2025.4.1310
16. Lian, F., Xing, B. (2017). Black carbon (biochar) in water/soil environments: Molecular structure, sorption, stability, and potential risk. *Environmental Science & Technology, 51*, 13517–13532. https://doi.org/10.1021/acs.est.7b02528
17. Liu, R., Wen, J., Song, J., et al. (2025). One-step and low-temperature KOH-K_2CO_3 synergistic activation of residual carbon from coal gasification slag for supercapacitor electrode material. *Ionics, 31*, 3607–3618. https://doi.org/10.1007/s11581-024-06044-9
18. Lyrshchikov, S.Y., Strizhak, P.A., Shevyrev, S.A. (2016). Thermal decomposition of coal and coal-enrichment wastes. *Coke and Chemistry, 59*, 264–270. https://doi.org/10.3103/S1068364X16070048
19. Muratov, M., Abdikamalova, A., Eshmetov, I., Mamataliyev, N., Xudoyberdiyev, N., Raximov, U., Ergashev, O., Seitnazarova, O., Mamajonov, B. (2025). Waste-derived activated carbons from phenol-formaldehyde and polystyrene: The role of PAN and alkali treatment. *Chemical Review and Letters, 8*, 981–1002. https://doi.org/10.22034/crl.2025.532995.1651
20. Muratov, M., Kurniawan, T.A., Eshmetov, R., Salikhanova, D., Eshmetov, I., Adizov, B., Onn, W. (2024). Promoting sustainability: Micellization and surface dynamics of recycled monoethanolamine surfactants. *Journal of Molecular Liquids.* https://doi.org/10.1016/j.molliq.2024.126010
21. Muratov, M.M., Abdikamalova, A.B., Seytnazarova, O.M., Najimova, N.B., Salikhanova, D.S., Eshmetov, I.D., Khaydarov, D.M., Abdirakhimov, A.K., Paygamov, R.A., Mamataliev, N.N. (2026). Acid-base activation of thermal power plant ash sludge and its adsorption properties towards heavy metals. *PPOR, 27*, 252–271. https://doi.org/10.62972/1726-4685.2026.1.252
22. Neme, I., Gonfa, G., Masi, Ch. (2022). Activated carbon from biomass precursors using phosphoric acid: A review. *Heliyon, 8*, 1–12. https://doi.org/10.1016/j.heliyon.2022.e11940
23. Nguyen, H.G.T., Toman, B., van Zee, R.D., et al. (2023). Reference isotherms for water vapor sorption on nanoporous carbon: Results of an interlaboratory study. *Adsorption, 29*, 113–124. https://doi.org/10.1007/s10450-023-00383-1
24. Wang, J., Kaskel, S. (2012). KOH activation of carbon-based materials for energy storage. *Journal of Materials Chemistry, 22*, 23710–23725. https://doi.org/10.1039/C2JM34066F)
25. Wang, J., Xu, B. (2023). Removal of radionuclide 99Tc from aqueous solution by various adsorbents: A review. *Journal of Environmental Radioactivity, 270*, 107267. https://doi.org/10.1016/j.jenvrad.2023.107267
26. Wang, K., Lin, G., Meng, J., et al. (2024). Textural properties prediction of KOH-activated carbon prepared from coal based on pyrolysis kinetics. *Waste Disposal & Sustainable Energy, 6*, 487–500. https://doi.org/10.1007/s42768-024-00204-3
27. Wang, S., Dai, G., Yang, H., Luo, Z. (2017). Lignocellulosic biomass pyrolysis mechanism: A state-of-the-art review. *Progress in Energy and Combustion Science, 62*, 33–86. https://doi.org/10.1016/j.pecs.2017.05.004
28. Weihong, Z., Bin, B., Guanyi, C., Longlong, M., Beibei, Y. (2019). Thermogravimetric characteristics and kinetics of sawdust pyrolysis catalyzed by potassium salt during the process of hydrogen preparation. *International Journal of Hydrogen Energy, 44*, 15863–15870. https://doi.org/10.1016/j.ijhydene.2019.01.060
29. Yahia, E.H., Serafin, J., Román-Martínez, M.C., Sreńscek-Nazzal, J., Dziejarski, B., Saidi, M., Ouzzine, M. (2025). Preparation of activated carbon from Moroccan argan press cake using KOH activation and its application for CO_2 adsorption. *Fuel, 393*, 134922. https://doi.org/10.1016/j.fuel.2025.134922
30. Yang, X., Wan, Y., Zheng, Y., He, F., Yu, Z., Huang, J., et al. (2019). Surface functional groups of carbon-based adsorbents and their roles in the removal of heavy metals from aqueous solutions: A critical review. *Chemical Engineering Journal, 366*, 608–621. https://doi.org/10.1016/j.cej.2019.02.119